Cancer Research

Hypoxia-Induced Epithelial-to-Mesenchymal Transition in Hepatocellular Carcinoma Induces an Immunosuppressive Tumor Microenvironment to Promote Metastasis

Long-Yun Ye[1,2], Wei Chen[1], Xue-Li Bai[1,2], Xing-Yuan Xu[1,2], Qi Zhang[1,2], Xue-Feng Xia[1], Xu Sun[1], Guo-Gang Li[1], Qi-Da Hu[1], Qi-Han Fu[1], and Ting-Bo Liang[1,2,3]

Abstract

Portal vein tumor thrombosis (PVTT) is a significant risk factor for metastasis in hepatocellular carcinoma (HCC) patients and is therefore associated with poor prognosis. The presence of PVTT frequently accompanies substantial hypoxia within the tumor microenvironment, which is suggested to accelerate tumor metastasis, but it is unclear how this occurs. Recent evidence has shown that the hypoxia-inducible factor HIF-1α induces epithelial-to-mesenchymal transition (EMT) in tumor cells to facilitate metastasis. In this study, we investigated whether hypoxia-induced EMT in cancer cells also affects immune cells in the tumor microenvironment to promote immunosuppression. We found that hypoxia-induced EMT increased the expression of the CCL20 cytokine in hepatoma cells. Furthermore, coculture of monocyte-derived macrophages with hypoxic hepatoma cells revealed that the expression of indoleamine 2, 3-dioxygenase (IDO) was induced in monocyte-derived macrophages in a CCL20-dependent manner. In turn, these IDO-expressing monocyte-derived macrophages suppressed T-cell proliferation and promoted the expansion of immunosuppressive regulatory T cells. Moreover, high CCL20 expression in HCC specimens was associated with PVTT and poor patient survival. Collectively, our findings suggest that the HIF-1α/CCL20/IDO axis in hepatocellular carcinoma is important for accelerating tumor metastasis through both the induction of EMT and the establishment of an immunosuppressive tumor microenvironment, warranting further investigation into the therapeutic effects of blocking specific nodes of this signaling network. *Cancer Res; 76(4); 818–30. ©2016 AACR.*

Introduction

Hepatocellular carcinoma is one of the most common malignancies worldwide with a poor prognosis (1–3). Metastasis is the leading cause of death in the majority of hepatocellular carcinoma patients, of which the overall five-year survival rate is merely 5% to 6% (4–6). The presence of a portal vein tumor thrombus (PVTT) is considered to be a strong predictor of metastasis and one of the most significant factors for a poor prognosis in hepatocellular carcinoma (7). Venous thrombosis is a major hallmark of metastatic hepatocellular carcinoma with 40% to 90.2% of advanced hepatocellular carcinoma patients reporting PVTT (7–10). The association of PVTT with hepatocellular carcinoma is mainly due to the highly vascular nature of hepatocellular carcinoma tumors (11, 12).

The tumor microenvironment plays an important role in cancer development and metastasis (13). Because of the rapid tumor cell growth, the tumor often outpaces its blood supply, leading to substantial hypoxia in the vicinity of hepatocellular carcinoma tumors (14). Hypoxia triggers overexpression of hypoxia-inducible factor 1α (HIF-1α), which has previously been shown to induce epithelial–mesenchymal transition (EMT) of cancer cells in breast cancer (15). During EMT, epithelial cells are converted into motile, invasive mesenchymal cells. EMT is frequently observed at the invasive front of advanced tumors and significantly correlates with metastasis in tumor progression (16–18). There is also increasing evidence for a functional relationship between EMT and macrophages, as both cell types are found at the invasive front of tumors (19, 20). However, it is unclear whether the EMT of cancer cells contributes to the immunosuppressive microenvironment in hepatocellular carcinoma.

Immune cells within the tumor microenvironment also play an important role in cancer development and metastasis. Monocytes can respond to environmental signals and differentiate into tumor supportive macrophages, which modulate the stroma to prompt tumor invasion and metastasis (21, 22). These monocyte-derived macrophages are the most abundant leukocytes that infiltrate the tumor microenvironment (23, 24). A subset of

[1]Department of Hepatobiliary and Pancreatic Surgery, The Second Affiliated Hospital, Zhejiang University School of Medicine, Hangzhou, P.R. China. [2]Key Laboratory of Cancer Prevention and Intervention, The Second Affiliated Hospital, Zhejiang University School of Medicine, Hangzhou, P.R. China [3]Collaborative Innovation Center for Cancer Medicine, Zhejiang University, Hangzhou, P.R. China.

Note: Supplementary data for this article are available at Cancer Research Online (http://cancerres.aacrjournals.org/).

L.-Y. Ye, W. Chen, and X.-L. Bai contributed equally to this article.

Corresponding Author: Ting-Bo Liang, Department of Hepatobiliary-Pancreatic Surgery, The Second Affiliated Hospital, Zhejiang University School of Medicine, 88 Jiefang Road, Hangzhou 310009, P.R. China. Phone: 8657-1873-15006; Fax: 8657-1873-15006; E-mail: liangtingbo@zju.edu.cn

doi: 10.1158/0008-5472.CAN-15-0977

monocyte-derived macrophages has increased expression of indoleamine 2, 3-dioxygenase (IDO), a rate-limiting enzyme required for degradation of tryptophan. These IDO^+ monocyte-derived macrophages can assist tumors by suppressing T-cell activation and proliferation through degradation of the essential amino acid tryptophan (25).

While the IDO^+ monocyte-derived macrophages play a vital role in establishing and maintaining an immunosuppressive tumor environment, the mechanism through which the microenvironment educates the monocytes and induces a tolerogenic state remains unclear. In this study, we explored that the interaction between hypoxia-induced EMT of cancer cells and monocyte-derived macrophages. We showed that increased levels of the CCL20 cytokine released from cancer cells significantly induced the expression of IDO in monocyte-derived macrophages, helping to form an immunosuppressive microenvironment to accelerate metastasis.

Materials and Methods

Patients and specimens

Tumor tissue samples were obtained from the Second Affiliated Hospital of Zhejiang University School of Medicine. Ninety patients with hepatocellular carcinoma underwent curative resection between 2007 and 2010, and samples from these patients were used for IHC and quantitative RT-PCR (qRT-PCR). This project was approved by the Ethics Committee of Second Affiliated Hospital of Zhejiang University School of Medicine. All samples were anonymously coded in accordance with local ethical guidelines (as stipulated by the Declaration of Helsinki), and written informed consent was obtained.

Cell culture and treatment

HL-7702 and human hepatoma cell line (Huh-7) were obtained from the Shanghai Institute for Biological Science (Shanghai, China). Hep-G2 cells were obtained from ATCC. They were maintained in DMEM supplemented with 10% FBS (Gibco) and 1% penicillin/streptomycin (Sigma). All cell lines were authenticated by a professional biotechnology company in 2015, and used in our previous study (26). Cells were exposed to hypoxia (1.0% O_2) in a hypoxic chamber (Thermal Tech) for the indicated time period.

Cells were transfected with HIF-1α siRNA #1 and #2 (Invitrogen) and negative control siRNA (nc-siRNA; GenePharma) at 100 nmol/L using Lipofectamine 2000 (Invitrogen) according to the manufacturer's instructions.

Chromatin immunoprecipitation assay and luciferase reporter assays

Putative hypoxia response element (HRE)-like sequences were identified in the *CCL20* promoter sequence using the regulatory sequence analysis tools (http://rsat.ulb.ac.be/rsat/). After treatment with 100 μmol/L $CoCl_2$ for 12 hours, Hep-G2 and Huh-7 cells were cross-linked and processed according to the Millipore EZ-ChIP Assay Kit protocol (Millipore). The mouse anti-human HIF-1α ChIP validated antibody (ab1, Abcam), and mouse IgG (negative control) were used. PCR analysis for *CCL20* was carried out using the primers (forward: 5′-GACCTTTGTATCGCTGTTAAT; reverse: 5′-AGTAGCAGCACTGACATCAAA) and the PCR products were analyzed by agarose gel electrophoresis.

The putative (AGAAGGCGTGTTGCCACA) HRE-like sequence synthesized by Hanbio was ligated into the pGL3-basic plasmid (Promega) to construct the *CCL20* promoter luciferase reporter plasmid. A VEGF reporter plasmid, containing a −1,005/+306 fragment from the human *VEGF* promoter, was constructed as described previously (27). Luciferase reporter assays were carried out in 24-well plates, and 250 ng of *CCL20* reporter plasmid or *VEGF* reporter plasmid was cotransfected with 750 ng *HIF-1α* plasmid (Vigene Bioscience CH886250) and 25 ng pRL-TK reporter plasmid (Millipore). Reporter activity was evaluated using the dual luciferase reporter system (Promega).

In vitro coculture model

Peripheral blood mononuclear cells (PBMC) were isolated by Ficoll density-gradient centrifugation. Monocytes were purified from PBMCs using anti-CD14 magnetic beads (Miltenyi Biotec), or fluorescence-activated cell sorting (FACS). Monocytes were cultured with cell lines expressing GFP at a ratio of 3:1 for 3 days. Then, the medium was changed to medium with CCL20 (100 ng/mL; PeproTech), medium with IFNγ (100 IU/mL; PeproTech), medium with fludarabine (50 μmol/L; Selleckchem), or the cells were directly cultured with hypoxic tumor cells for one day. After one day, fresh medium was added and the cells were cultured for another day. Then, we sorted the GFP-expressing hepatoma cells from the non-GFP–expressing monocytes using FACS (Supplementary Fig. S3C). The supernatants were harvested and kynurenine was detected (28).

In vitro T-cell culture models

Circulating T cells were purified using the Pan T Cell Isolation Kit II (Miltenyi Biotec) or FACS sorting. Autologous or treated monocytes were pretreated with 10 μg/mL mitomycin C (Sigma) for 30 minutes, washed twice, and cocultured for 7 days with polyclonal-stimulated (10 μg/mL anti-CD3 and 10 μg/mL anti-CD28) and prelabeled CFSE T cells at a ratio of 1:10 in the presence or absence of 100 μmol/L (1-MT; Sigma). Functional assays were carried out using the regulatory T cell (T_{reg}) suppression inspector (Miltenyi Biotec), with five ratios of T_{eff}: T_{reg} cells (0:1, 1:0, 1:1, 4:1 and 8:1).

Flow cytometry

All antibodies used were purchased from Biolegend unless specified otherwise. Macrophages were stained with fluorochrome-conjugated mAbs for CD14 (HCD14), CD16 (3G8), CD45(HI30), CD163 (GHI/61), CD206 (15-2), or HLA-DR (L243) with a control antibody. T cells were left untreated or were stimulated at 37°C for 5 hours with Cell Activation Cocktail (Biolegend). Thereafter, cells were stained with CD3 (145-2C11), CD4 (RM4-5), CD8 (SK1), CD25 (BC96), CD127 (A019D5), IFNγ (4S.B3), Foxp3 (206D), and IL2 (MQ1-17H12). Cell sorting was performed on a FACSAria II (BD Biosciences) and flow cytometric analysis was performed on a Canto-II (BD Biosciences). We used the Intracellular Cytokine Staining Kit from BD Pharmingen, and the transcriptional factor staining was performed using the Fix/Perm Kit (eBioscience).

ELISA

The supernatants were collected and stored at 4°C. Concentrations of CCL20, IL10, IL12, IL6, and VEGF in the conditioned media were detected using ELISA kits (R&D Systems, Inc.).

Immunofluorescence and IHC

For immunofluorescence staining, frozen samples of 5-μm tissue sections or treated cells were stained with anti-E-cadherin (1:100; Cell Signaling Technology), anti-vimentin (1:100; Cell Signaling Technology), IDO (1:100; Millipore), or CCL20 (1:200; Abcam) at 4°C overnight, followed by incubation with goat anti-rabbit or mouse FITC- or PE-conjugated (1:1,000; Liankebio). Positive cells were quantified by confocal microscopy and analyzed by ImagePro Plus software. Staining without primary antibodies were used as negative controls.

Paraffin-embedded hepatocellular carcinoma tissue samples were cut into 5-μm sections and processed for IHC (29). The slides were incubated with human anti-CCL20 (1:1,000) or HIF-1α (1:1,000) antibodies. We defined samples without any staining as 1 score. Other samples were defined as low (2 scores), medium (3 scores), or high (4 scores) levels of expression. The scoring system is illustrated using representative samples of each score in Supplementary Fig. S6 and was evaluated by two independent pathologists.

Immunoblotting and antibodies

Western blot analysis was performed to detect the levels of CCL20 (ab9829, Abcam), IDO (ab156787, Abcam), STAT1 (ab2415, Abcam), p-STAT1 (ab29045, Abcam), STAT3 (9139, Cell Signaling Technology), p-STAT3 (9145, Cell Signaling Technology), E-cadherin (3195, Cell Signaling Technology), vimentin (5741, Cell Signaling Technology), Snail (3879, Cell Signaling Technology), and HIF-1α (NB100-105, Novusbio). The proteins were extracted and separated by SDS-PAGE then transferred to polyvinylidene difluoride membranes (Millipore). Membranes were incubated overnight at 4°C with specific primary antibodies. The next day, membranes were further incubated with secondary antibodies and visualized using ChemiDoc XRS System (Bio-Rad Laboratories) or X-ray film (Kodak).

Quantitative reverse transcription PCR

Tumor sample or cells were lysed as previous described. qRT-PCR was performed on the ABI 7900 Prism HT (Applied Biosystems), followed by melting curve analysis. The ΔC_t method was used to assess the gene expression fold change among groups. Three independent experiments were performed.

Statistical analysis

Statistical calculations were performed using Prism 5 software (GraphPad). Data were expressed as mean and SD, unless otherwise indicated. Continuous variables were evaluated using an unpaired Student *t* test for comparisons between two groups. Categorical variables were compared using a χ^2 test (or Fisher exact test). Multivariate analysis was performed using forward stepwise logistic regression analysis. Survival analysis was conducted using the Kaplan–Meier method with the log-rank test. Two-sided tests were performed with a $P < 0.05$ indicating statistical significance.

Results

HIF-1α is positively associated with PVTT in hepatocellular carcinoma patients

To evaluate the clinical outcomes of PVTT in hepatocellular carcinoma patients, we analyzed the survival of 90 hepatocellular carcinoma patients who received surgery in the Second Affiliated Hospital of Zhejiang University School of Medicine in China. The results showed that 21 patients within PVTT group had a significantly worse prognosis than the other patients (Fig. 1A). As HIF-1α is one of the most potent proteins linked to liver metastasis and tumor progression, we examined *HIF-1α* mRNA level in normal livers, tumors without PVTT, and tumors with PVTT ($n = 21$ in each group; Fig. 1B). *HIF-1α* mRNA level was significantly higher in the group of tumors with PVTT. Moreover, we found significantly strong nuclear staining for HIF-1α in the tumors with PVTT (Fig. 1C and 1D).

HIF-1α induces EMT in hepatocellular carcinoma cell lines

We examined the potential for hypoxia to induce EMT in hepatocellular carcinoma cell lines, Huh-7 and Hep-G2. After exposure to 1.0% oxygen for 24 hours, the morphology of the Huh-7 and Hep-G2 cells became significantly stretched and elongated (Fig. 1E). The epithelial biomarker E-cadherin was downregulated, while simultaneously the mesenchymal biomarkers vimentin and Snail increased (Fig. 1F). In addition, immunofluorescence showed weaker E-cadherin membrane localization and stronger intracytoplasmic localization of vimentin (Fig. 1G). These results are all typical of events that occur during EMT of tumor cells.

HIF-1α induces the expression of the cytokine CCL20 by mesenchymal cancer cells

To investigate whether there was a change in the cytokine profile associated with hypoxia-induced EMT of cancer cells, the hypoxic medium from Hep-G2 cells was analyzed using the RayBio Human Cytokine Antibody Array (AAH-CHE-1; Fig. 2A). The expression of six cytokines [CCL2, CCL20, CXCL1 (GROα), CXCL8 (IL-8), CXCL9, and CXCL16] increased significantly compared with the condition medium of untreated Hep-G2 cells, and the levels of CCL20 increased most dramatically. We used qRT-PCR to confirm an increase in *CCL20* gene expression at 16 and 24 hours in both Huh-7 cells and Hep-G2 cells under hypoxic conditions (Fig. 2B).

To confirm whether the HIF-1α was responsible for this change in cytokine levels, HIF-1α accumulation and CCL20 levels were examined over time in Huh-7 and Hep-G2 cells exposed to 1% oxygen (Fig. 2C). HIF-1α reached a peak at 16 hours, and then gradually declined, which was consistent with the dynamic change in CCL20 gene expression. However, the protein levels of CCL20 did not reach a maximum until 24 hours. Therefore, there may be a time delay between HIF-1α–induced gene expression and secreted protein levels for CCL20. Knockdown of HIF-1α by siRNA (100 nmol/L) in Hep-G2 and Huh-7 cells resulted in a significant decrease in the expression of CCL20 compared with the control (ncRNA at 100 nmol/L; Fig. 2D). After HIF-1α knockdown, there was no upregulation of EMT markers observed either by Western blot or immunofluorescence under hypoxic conditions. Furthermore, the Transwell assay showed that HIF-1α knockdown prevented hypoxic Huh-7 or Hep-G2 cells passing through the Matrigel-coated membranes (Supplementary Fig. S1A–S1C).

To understand whether there was direct association between HIF-1α and CCL20, we overexpressed HIF-1α (using a *HIF-1α* plasmid) and found that CCL20 dramatically increased both in Hep-G2 and Huh-7 cells (Fig. 2E). To further confirm that the *CCL20* gene is regulated directly by hypoxia through a HRE [(A/G)CGTG); refs. 30–32], high-scoring HRE-like sequences in the *CCL20* gene promoter were identified by

bioinformatics analysis. Moreover, a ChIP assay using an anti-HIF-1α showed that the putative HRE in the promoter of the *CCL20* gene (AGAAGGCGTGTTGCCACA) was captured (Fig. 2F). To determine whether the putative HRE plays a functional role in hypoxia-dependent transcriptional activation, we cotransfected cells with the *HIF-1α* plasmid and a *CCL20* or *VEGF* luciferase reporter. Inducibility of the *CCL20* reporter by *HIF-1α* overexpression was compared with that of *VEGF* reporter, which contains a functional HIF-1α–binding site. We detected a substantial, significant increase of *CCL20* promoter transactivation (approximately 5–10 fold relative to control cells) in response to HIF-1α overexpression. This result confirms that the putative HRE (AGAAGGCGTGTTGCCACA) in *CCL20* was activated by HIF-1α (Fig. 2G). Taken together, these results suggest that a functional HRE motif exists in the promoter fragment of the *CCL20* gene that mediates hypoxia-dependent CCL20 expression.

To evaluate the potential relationship of HIF-1α and CCL20 in the tumor microenvironment, we analyzed their expression in adjacent sections of hepatocellular carcinoma tissues by staining for HIF-1α and CCL20 (Supplementary Fig. S2). HIF-1α was expressed at higher levels at the invasive front (Supplementary Fig. S2). We observed the same gradient for CCL20 with higher levels at the tumor edge, where cancer cells displayed more mesenchymal features and expressed high levels of HIF-1α, compared with the center of the tumor (Supplementary Fig. S2). These data indicated that hypoxia-induced mesenchymal cancer cells secreted more CCL20 at the invasive front due to increased levels of HIF-1α.

Tumor-derived CCL20 upregulates IDO expression in monocyte-derived macrophages

Tumor microenvironments recruit monocytes from blood, and educate them, converting them into tumor supportive macrophages. Previous studies used the tumor culture supernatants from hepatoma cells to induce the macrophages (22, 33). However, this model may not accurately reflect the effects of cell-to-cell contacts, which are important for cell surface marker function. Therefore, in this study, we cocultured isolated monocytes directly with hepatoma cells (Huh-7 and Hep-G2). After 72 hours, the monocytes cocultured with hepatoma cells, but not with HL-7702, exhibited a high expression of CD206 and CD163 (Supplementary Fig. S3A). Moreover, the levels of HLA-DR were reduced in monocytes exposed to hepatoma cells compared with HL-7702 (Supplementary Fig. S3A). The activation of suppressive monocyte-derived macrophages was also confirmed by IL10, IL12, IL6, and VEGF cytokine production (Supplementary Fig. S3B).

To further identify the effect of the hypoxia-induced cytokines in the tumor microenvironments, we directly cultured monocyte-derived macrophages with hypoxic hepatoma cells and then sorted the monocyte-derived macrophages from the tumor cells. We found that the expression of IDO increased in the monocyte-derived macrophages (Fig. 3A). As Lutz and colleagues reported (34), $CD14^+$ monocytes are heterogeneous, and include different subsets of monocytes. Therefore, we sorted the major subset (the classical $CD14^{++}CD16^-$ subset) from the two minor $CD16^+$ subsets (the intermediate $CD14^{++}CD16^+$ and the nonclassical $CD14^+CD16^{++}$ subsets). Consistent with a previous report (35), the nonclassical $CD14^+CD16^{++}$ monocytes expressed the lowest levels of CD163 and CD206 compared with the other two subsets, which may be partially due to the proinflammatory properties of this subset (36). When we cocultured these three subsets of monocytes with tumor cells, the expression of CD163 and CD206 increased considerably (Fig. 3B). Furthermore, we sorted the three different subsets of cells and cocultured them separately with hypoxic hepatoma cells. We found that the expression of IDO was almost the same among the three subsets (Fig. 3C). Therefore, all three subsets of monocytes can be affected by the coculture system.

Next, we extensively explored which cytokine was responsible for this effect, and found that CCL20, and not CCL2, CXCL1, CXCL8, CXCL9, or CXCL16, significantly induced the expression of IDO in monocyte-derived macrophages (Fig. 3D). The expression of IDO was confirmed by confocal microscopy results (Supplementary Fig. S4A). In parallel with IDO expression, we observed an increase in its catalyzed product (kynurenine) in the culture supernatant (Supplementary Fig. S4B). To further confirm this, we added the neutralizing anti-CCL20 antibody to the hypoxic medium and found that the expression of IDO was reduced to almost same level as the control (Fig. 3E).

We also evaluated CCL20 and IDO levels in human hepatocellular carcinoma tissue. Immunofluorescence of frozen sections showed that most CCL20 surrounded IDO at the invasive front of the tumor (Fig. 3I). We measured mRNA levels of *IDO* by qRT-PCR, using the same set of tissue samples shown in Fig. 1A, and found that *IDO* (Fig. 3F) and *CCL20* (Fig. 3G) mRNA significantly increased in the group of tumors with PVTT. Furthermore, the *IDO* mRNA was positively associated with the *CCL20* mRNA level in tumors with PVTT group (Fig. 3H). However, there was no significant association between *IDO* and *CCL20* expression in the group with normal liver tissue (Supplementary Fig. S5A) and the group with tumors without PVTT (Supplementary Fig. S5B). Collectively, these results provided strong support for our hypothesis that the elevation of IDO was likely the result of the elevation of CCL20 as the etiologic factor in the development of tumor thrombus.

Phosphorylation of STAT1 is required for upregulation of IDO expression

Previous studies indicated that JAK–STAT pathway and NF-κB signaling pathways were involved in the regulation of IDO expression in macrophages and dendritic cells (DC). STAT1 activation was accepted as the canonical mechanism for mediating the induction of IDO expression by IFNγ. However, the molecular mechanism behind the upregulation of IDO expression in monocyte-derived macrophages after CCL20 treatment is still unclear. Therefore, we studied the expression and phosphorylation of STAT1, STAT3, and P65 (Fig. 4A). The treatment of CCL20 significantly induced the expression and nuclear translocation of phosphorylated-STAT1 (pSTAT1) in monocyte-derived macrophages (Fig. 4B and D). Fludarabine, the specific antagonist of STAT1 phosphorylation, downregulated expression of pSTAT1 and IDO proteins (Fig. 4C), and inhibited STAT1 nuclear translocation (Fig. 4D). These results suggest that CCL20-induced expression of IDO might be a result of activation of phosphorylation and nuclear translocation of STAT1.

IDO^+ monocyte-derived macrophages induce T cell dysfunction via an IDO-dependent manner

To define whether CCL20-treated monocyte-derived macrophages exhibited an immunosuppressive function, we cocultured

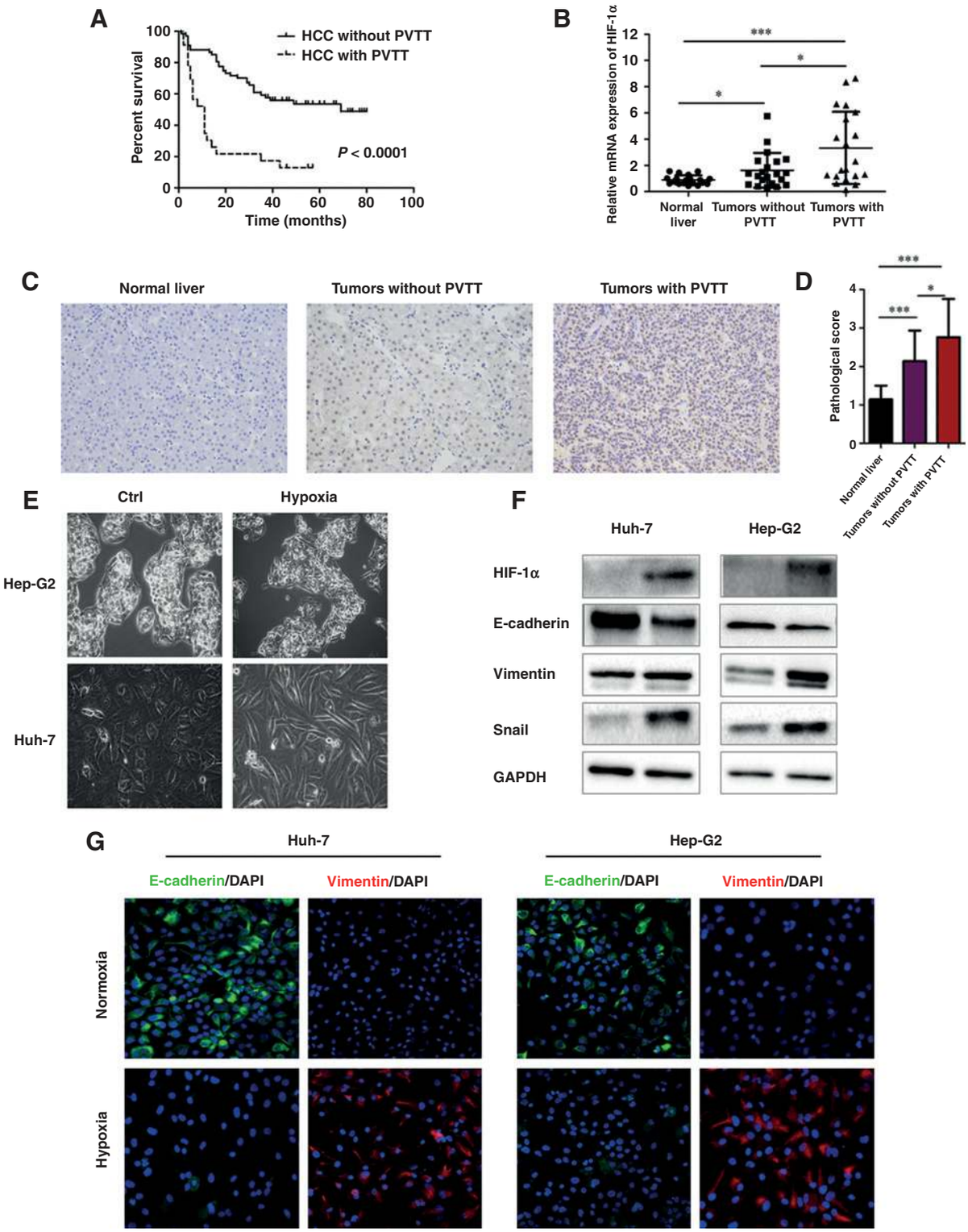

Figure 1.
HIF-1α is positively associated with PVTT development in hepatocellular carcinoma patients. A, the cumulative overall number of hepatocellular carcinoma patients with PVTT compared with those without PVTT over time, estimated using the Kaplan–Meier method. B, relative mRNA levels of *HIF-1α* measured by qRT-PCR and normalized to β-actin, in normal livers, and in hepatocellular carcinoma tumors without and with PVTT. Data are expressed as means ± SD and compared using the unpaired *t* test (*, $P < 0.05$; **, $P < 0.01$; ***, $P < 0.001$). (*Continued on the following page.*)

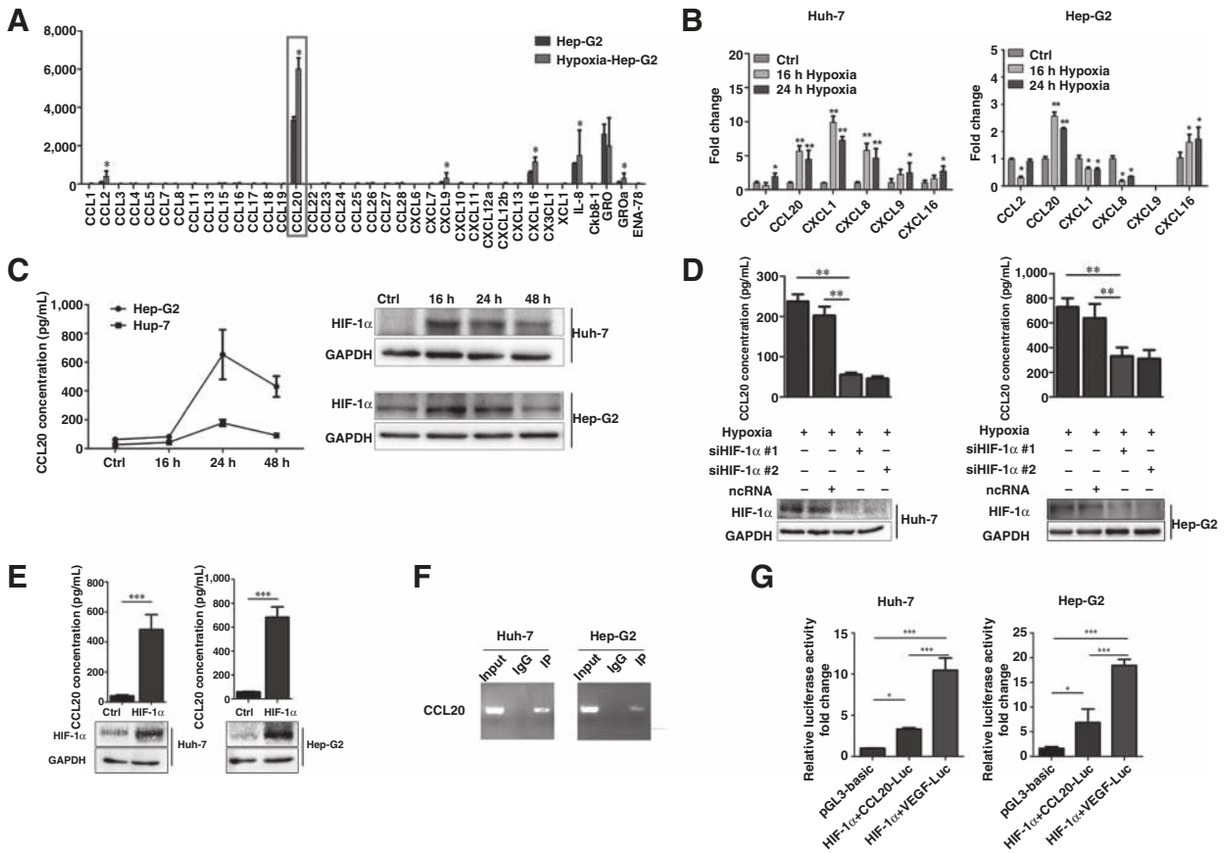

Figure 2.
Relative levels of CCL20 increase most dramatically among the cytokines under hypoxia. A, cytokine array from the condition medium of Hep-G2 cells and Hep-G2 induced to undergo EMT by culturing for 24 hours in 1.0% oxygen. The relative signal intensity of each of the indicated cytokines is shown. B, relative levels of *CCL2*, *CCL20*, *CXCL1*, *CXCL8*, *CXCL9*, and *CXCL16* in Huh-7 and Hep-G2 as measured by qRT-PCR (normalized to β-actin) after 0, 16, and 24 hours of culturing in 1.0% oxygen. C, CCL20 concentration (detected by ELISA) and HIF-1α accumulation (detected by Western blot analysis) in Huh-7 and Hep-G2 cells exposed to 1% oxygen from 0 to 48 hours. GAPDH was used as loading control for the Western blot analysis. D, expression of CCL20 after HIF-1α knockdown by siRNA #1 and #2 (100 nmol/L) compared with controls (ncRNA at 100 nmol/L) in Hep-G2 and Huh-7 cells. HIF-1α knockdown was confirmed using Western blot analysis, with GAPDH as a loading control. E, expression of CCL20 (detected by ELISA) and HIF-1α (detected by Western blot analysis) in Huh-7 and Hep-G2 cells after transfection with the *HIF-1α* plasmid. GAPDH was used as loading control for the Western blot analysis. F, ChIP analysis using anti-HIF-1α to ascertain the existence of the HRE in the promoter of the *CCL20* gene. PCR results showing that one fragment containing the putative HRE could be precipitated after treatment of Hep-G2 and Huh-7 cells with $CoCl_2$ 100 μmol/L for 12 hours. G, luciferase activities of *CCL20* or *VEGF* cotransfected with *HIF-1α* plasmid. Results in A–G are expressed as means ± SD of at least three separate experiments and compared using the unpaired *t* test (*, $P < 0.05$; **, $P < 0.01$; *** $P < 0.001$).

monocyte-derived macrophages with T cells to detect proliferation and cytokine production. Compared with controls, hypoxic tumor-treated monocyte-derived macrophages slightly inhibited the proliferation of T cells. The addition of CCL20-treated IDO$^+$ monocyte-derived macrophages further enhanced the inhibition (Fig. 5A and B). When IDO activity was blocked with the competitive inhibitor 1-MT, the effect of T-cell inhibition was attenuated. On the other hand, CCL20-treated IDO$^+$ monocyte-derived macrophages significantly decreased secretion of IFNγ both in CD4$^+$ and CD8$^+$ T cells (Fig. 5C and D). As expected, 1-MT suppressed the inhibitory effect of monocyte-derived macrophages on IFNγ secretion.

We also examined whether the CCL20-treated IDO$^+$monocyte-derived macrophages influence the generation of immunosuppressive T_{reg}-like cells. Autologous-sorted CD4$^+$CD25$^-$ effector T cells were cocultured with IDO$^+$ monocyte-derived macrophages. After 7 days, we found high expression of Foxp3 in T cells (Fig. 5E–G). Foxp3 was significantly induced in the

(*Continued.*) *HIF-1α* mRNA was undetectable in one normal liver tissue and one tumor with PVTT. C, IHC staining showing the accumulation of HIF-1α in normal liver, tumor without PVTT, and tumor with PVTT. Representative images at ×200 magnification from one set of the samples are shown. D, statistical analysis of the pathologic scores of HIF-1α in the various groups. Data are expressed as means ± SD and compared using the unpaired *t* test (*, $P < 0.05$; **, $P < 0.01$; ***, $P < 0.001$). E, bright field microscopy showing the morphologic changes that occur when Huh-7 and Hep-G2 cells are cultured for 24 hours in 1.0% oxygen. F, detection of HIF-1α, E-cadherin, vimentin, and Snail proteins using Western blot analysis. GAPDH was used as loading control. One of three representative Western blots is shown. F, immunofluorescence staining showing that the staining of E-cadherin (green) and vimentin (red) changes under normal and hypoxic conditions in both Huh-7 and Hep-G2 cells.

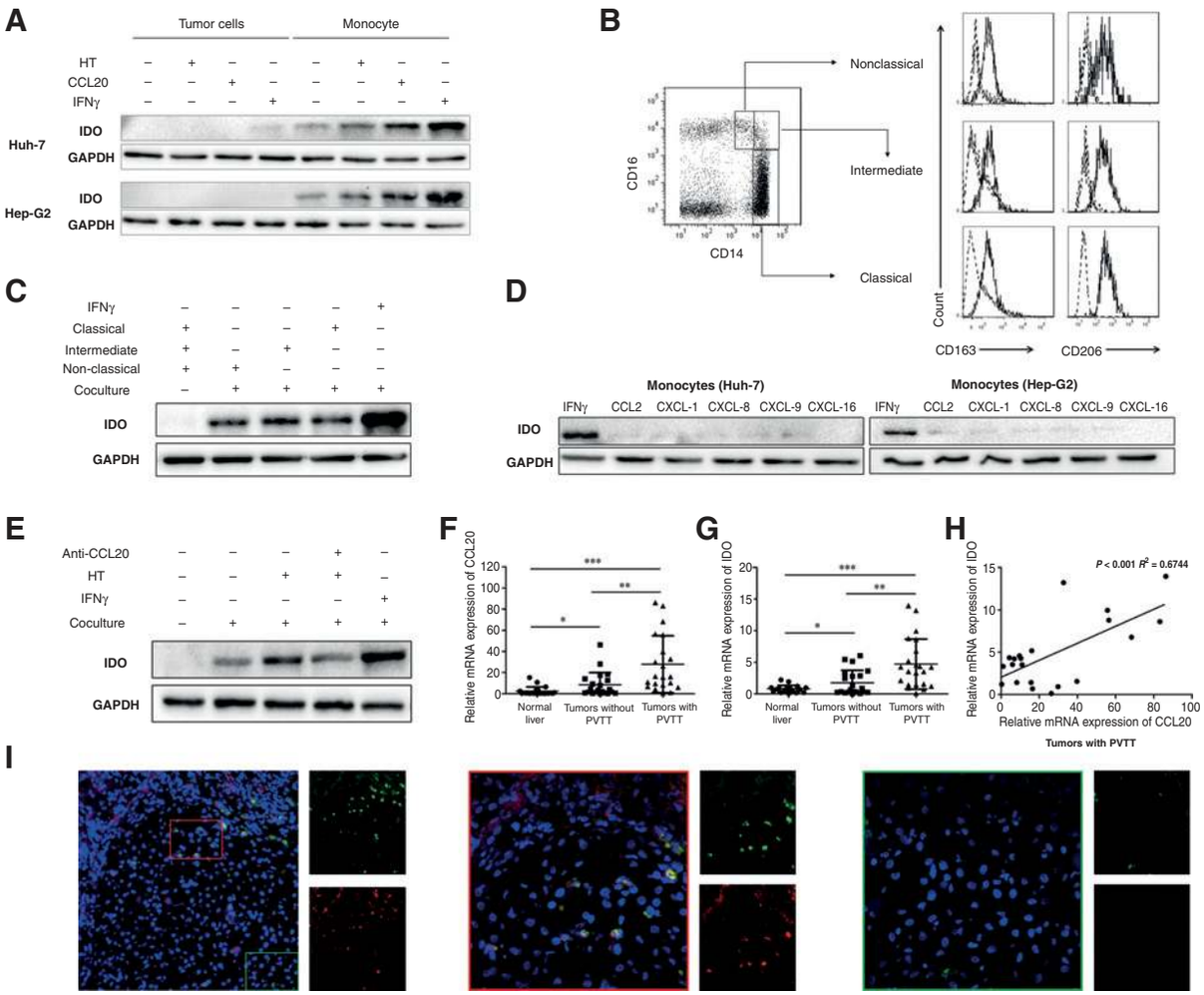

Figure 3.
Tumor-derived CCL20 upregulates IDO expression in monocyte-derived macrophages. A, $CD14^+$ monocytes cocultured with Huh-7 and Hep-G2 cells in the presence or absence of hypoxic tumor (HT) cells, CCL20, or IFNγ. IDO protein was detected by Western blot analysis in each case, with GAPDH used as a loading control. Western blot results are from at least 10 individual experiments. B, three subsets of $CD14^+$ monocytes were sorted and cocultured with Huh-7 and Hep-G2 cells, and the expression of CD163 and CD206 was analyzed by flow cytometry (solid line) compared with corresponding cells before culture (dash line). C, the expression of IDO was detected in the three different subsets of monocytes after coculture with hypoxic tumor (HT). D, levels of various cytokines in $CD14^+$ monocytes cocultured with Huh-7 and Hep-G2 cells as detected by Western blot analysis. E, the expression of IDO protein after using the neutralizing antibody for CCL20 as detected by Western blot analysis. F and G, relative mRNA levels of *CCL20* and *IDO*, measured by qRT-PCR and normalized β-actin, in tissue specimens from the same set of patients from Fig. 1B. Data are expressed as means ± SD of three independent experiments and were compared using an unpaired *t* test (*, $P < 0.05$; **, $P < 0.01$; ***, $P < 0.001$). *CCL20* and *IDO* mRNA was undetectable in one normal liver tissue. H, the correlation between *IDO* and *CCL20* expression for each individual in the tumor with PVTT group assessed by linear regression. I, physical contact between $CCL20^+$ cells (green) and IDO^+ cells (red) in the invading edge of cancer in hepatocellular carcinoma samples. One of 10 representative images from each set of samples is shown. Magnification at ×200 for the left image and ×400 for the two inset boxes (red and green). One of three representative results is shown in B–E.

$CD4^+CD25^+$ cells other than in $CD4^+CD25^-$ cells (Fig. 5G). To further determine the function of these T_{reg}-like cells, we sorted the $CD4^+CD25^+CD127^-$ cells from the coculture system. We cultured the sorted autologous $CD4^+CD25^-$ cells with the T_{reg} Suppression Inspector (Miltenyi Biotec) at five different ratios of T_{eff} cells: T_{reg} cells (i.e., 0:1, 1:0, 1:1, 4:1, and 8:1). We found that the proliferation of T cells was significantly inhibited by the T_{reg} -like cells compared with the control (Fig. 5H and I). These findings suggest that IDO^+ monocyte-derived macrophages exert an immunosuppressive effect on T cells in an IDO-dependent manner.

High amounts of CCL20 predict poor patient survival

To investigate the clinical relevance of elevated CCL20 levels in hepatocellular carcinoma cancer patients, we performed immunohistochemical staining in the 90 hepatocellular carcinoma samples. We divided patients into "low" and "high" expression groups, based on the median value of CCL20 levels, to assess the association of expression of CCL20 with clinical characteristics (Fig. 6A; Supplementary Fig. S6). We found that the high expression of CCL20 was significantly correlated with the tumor PVTT group ($P = 0.030$; Supplementary Table. S1). There was a significant inverse correlation of tumor CCL20 expression with both

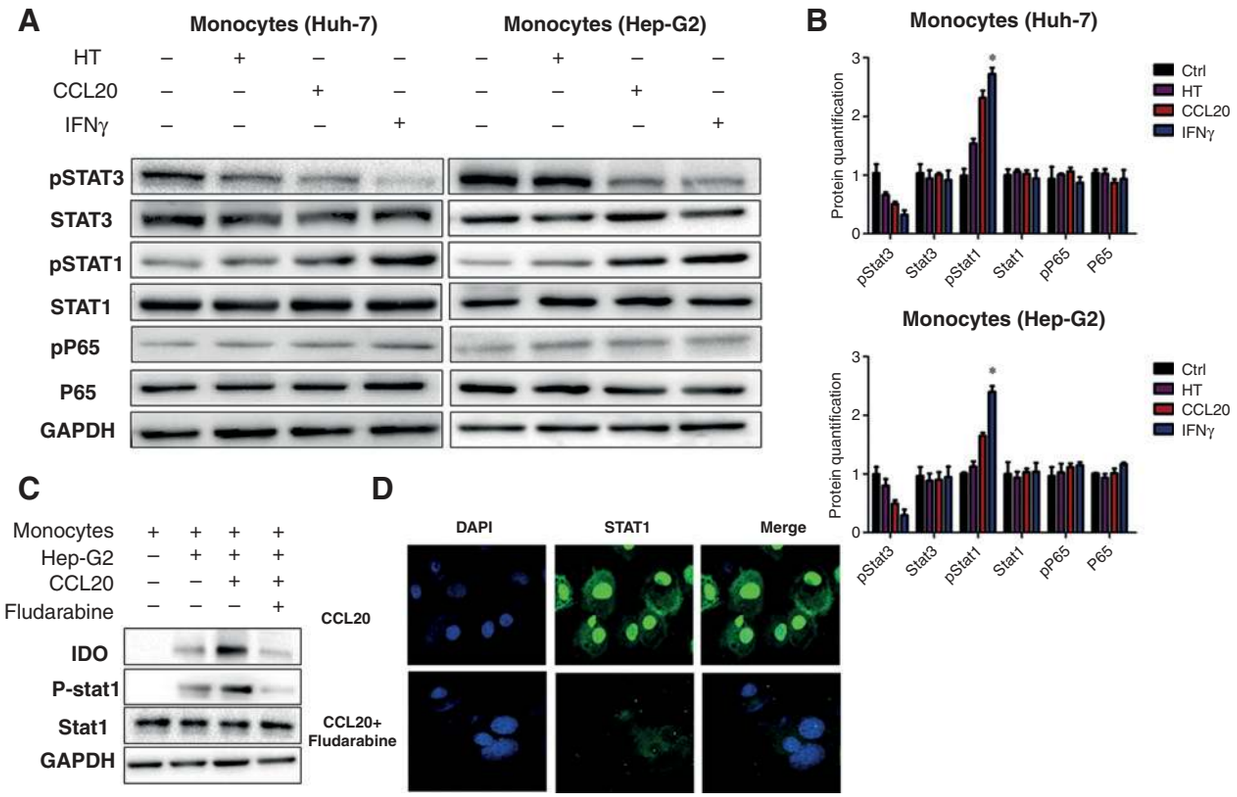

Figure 4.

Phosphorylation of STAT1 is required for upregulation of IDO expression. A, protein levels of pSTAT3, STAT3, pSTAT1, STAT1, pP65, and P65 in $CD14^+$ monocytes cocultured with Huh-7 and Hep-G2 cells in the presence or absence of hypoxic tumor (HT) cells, CCL20, or IFNγ as detected by Western blot analysis. GAPDH was used as a loading control. B, statistical analysis of the pSTAT3, STAT3, pSTAT1, STAT1, pP65, and P65 protein levels in the various groups is shown. Protein levels were quantified by densitometry, corrected for the sample load based on GAPDH expression, and expressed as fold-increase or decrease relative to the control lane. Data are expressed as means ± SD and were compared using the unpaired *t* test (*, $P < 0.05$; **, $P < 0.01$; ***, $P < 0.001$). C, protein levels of pSTAT1, STAT1, and IDO in $CD14^+$ monocytes cocultured with Hep-G2 cells, CCL20, or fludarabine (a STAT1 antagonist at 50 μmol/L) as detected by Western blot analysis. D, immunofluorescent images showing the nuclear location of STAT1 in monocytes after treatment of fludarabine (50 μmol/L) in the presence of CCL20. One of three representative results is shown in A, C, and D.

disease-free survival ($P = 0.0197$; Fig. 6B) and overall survival ($P = 0.0083$; Fig. 6C). Univariate and multivariate analysis showed that α-fetoprotein (AFP), tumor PVTT, and elevated CCL20 expression, were independent factors for overall survival ($P < 0.05$; Supplementary Table. S2).

We also analyzed the relationship between CCL20 and IDO expression in hepatocellular carcinoma patients with or without vascular invasion from National Center for Biotechnology Information Gene Expression Omnibus database (GSE20238; ref. 37). The database includes a total of 91 hepatocellular carcinoma patients and the associated vascular invasion data for 79 patients. Our analysis showed that the CCL20 levels significantly correlated with IDO in patients with vascular invasion ($P = 0.0443$; Fig. 6D). In contrast, no significant association was observed in patients without vascular invasion ($P = 0.7949$; Fig. 6E). These data strongly suggest that increased tumor CCL20 abundance is a significant and independent predictor of poor survival in hepatocellular carcinoma patients.

Discussion

Over the past decade, much research into hepatocellular carcinoma has focused on the cancer cells themselves, without taking into account the unique but complex tumor microenvironment. Hypoxia in the tumor microenvironment plays an important role in driving cell metastasis (38, 39). Our study demonstrated that PVTT can cause substantial hypoxia in hepatocellular carcinomas compared with the hepatocellular carcinomas without PVTT. However, whether the reverse is true (i.e., that different levels of HIF-1α directly induce the formation of PVTT) remains unclear. Indeed, some patients with high HIF-1α expression still existed in the PVTT− group compared with the PVTT+ group (Fig. 1B). Moreover, based on our findings, we cannot conclude whether HIF-1α has on–off or a more graduated effect on PVTT formation.

In response to hypoxia, HIF-1α is known to accumulate and induce EMT in tumor cells to facilitate metastasis (40). During EMT, tumor cells acquire cell motility, with decreased adhesive ability and a rearranged cytoskeleton (40, 41). EMT is also thought to have another function: to create an immunosuppressive microenvironment by educating the infiltrating immune cells (42). We examined whether a change in the secretory cytokine profile during EMT may be the key factor for educating immune cells in the microenvironment. We found hypoxia-induced mesenchymal cancer cells elevated the levels of CCL20 in the

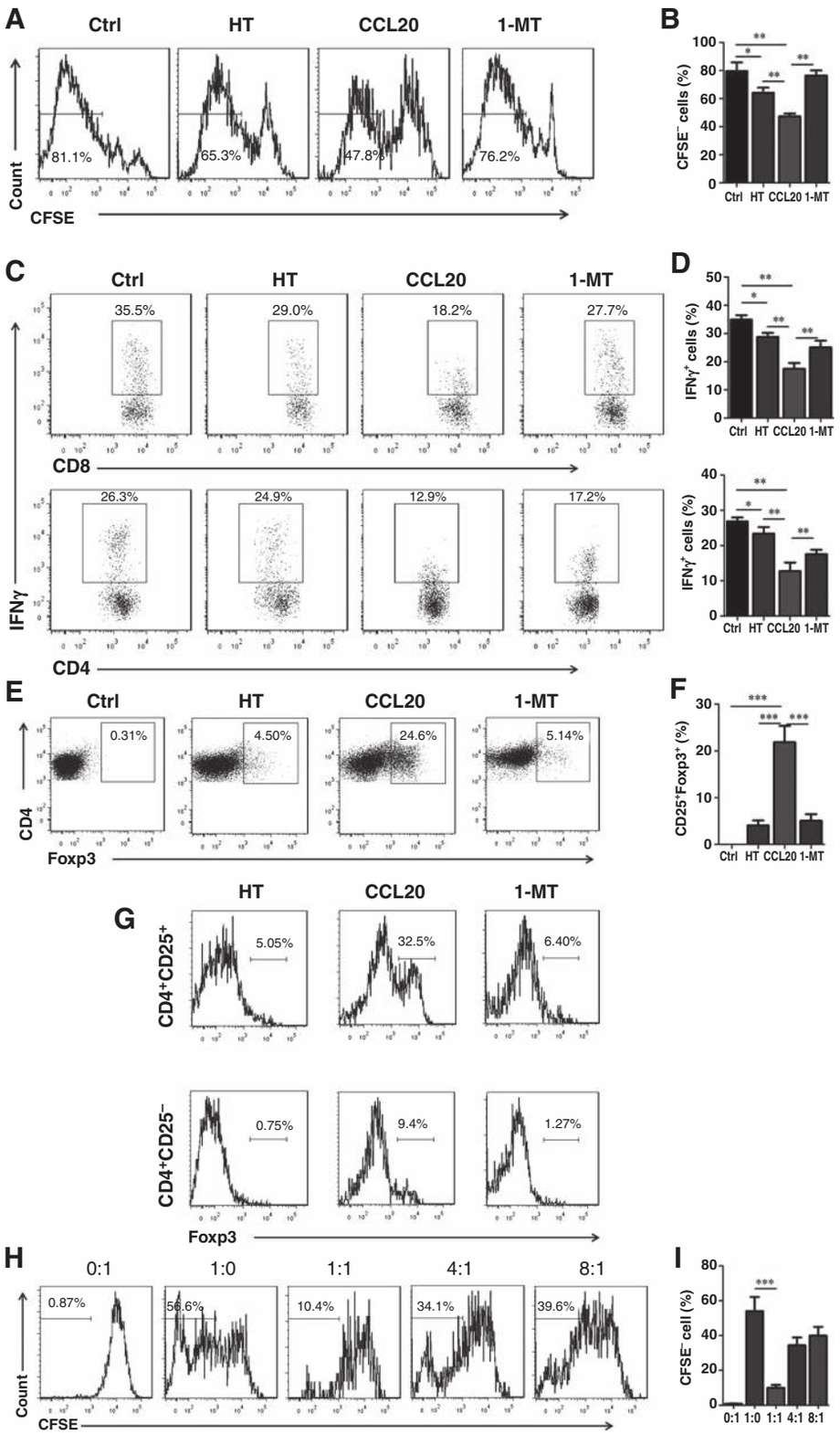

Figure 5.
IDO$^+$ monocyte-derived macrophages induce T-cell dysfunction in an IDO-dependent manner. Monocyte-derived macrophages were cocultured with polyclonal-stimulated (10 μg/mL anti-CD3 and 10 μg/mL anti-CD28) autologous T cells at a ratio of 1:10 in the presence or absence of the IDO inhibitor (1-MT) at 100 μmol/L. CFSE-prelabeled T-cell proliferation was evaluated on day 7 by flow cytometry. A, the percentage of T cells without addition of monocytes in the control group compared with the percentage in the samples cocultured with hypoxic tumor (HT) cells, CCL20, or 1-MT. B, statistical analysis on the percentage of proliferated T cells (CFSE$^-$) in the various groups. C, IFNγ production in CD4$^+$ and CD8$^+$ cells cocultured with hypoxic tumor (HT)-treated monocyte-derived macrophages, CCL20-treated IDO$^+$ monocyte-derived macrophages, or 100 μmol/L 1-MT, showing that IDO$^+$ monocyte-derived macrophages significantly decreased secretion of IFNγ both in CD4$^+$ and CD8$^+$ T cells. D, statistical analysis of the percentage of IFNγ$^+$ T cells in the various groups. E, sorted CD4$^+$CD25$^-$ effector T cells cocultured with monocyte-derived macrophages in the presence or absence of 100 μmol/L 1-MT. F, statistical analysis of the percentage of CD4$^+$Foxp3$^+$ T cells in the various groups. G, the percentage of Foxp3$^+$ cells was analyzed after gating cells CD4$^+$CD25$^+$ cells (top) or CD4$^+$CD25$^-$ cells (bottom) by flow cytometry. H, T_{reg} cell suppression assay comparing T-cell functions with five ratios of T_{eff}: T_{reg} cells (0:1, 1:0, 1:1, 4:1, and 8:1). I, statistical analysis of the percentage of CFSE$^-$ T cells in the various groups. Data in A–I show means ± SD of five separate experiments and were compared using the unpaired *t* test (*, $P < 0.05$; **, $P < 0.01$; ***, $P < 0.001$).

microenvironment. Moreover, we identified a functional HRE within the *CCL20* promoter for the first time. Therefore, we propose that hypoxia induces HIF-1α, which interacts with this HRE to stimulate the transcription of CCL20. Together, our results suggest that CCL20 expression is under the direct control of HIF-1α via a HRE in the *CCL20* gene promoter.

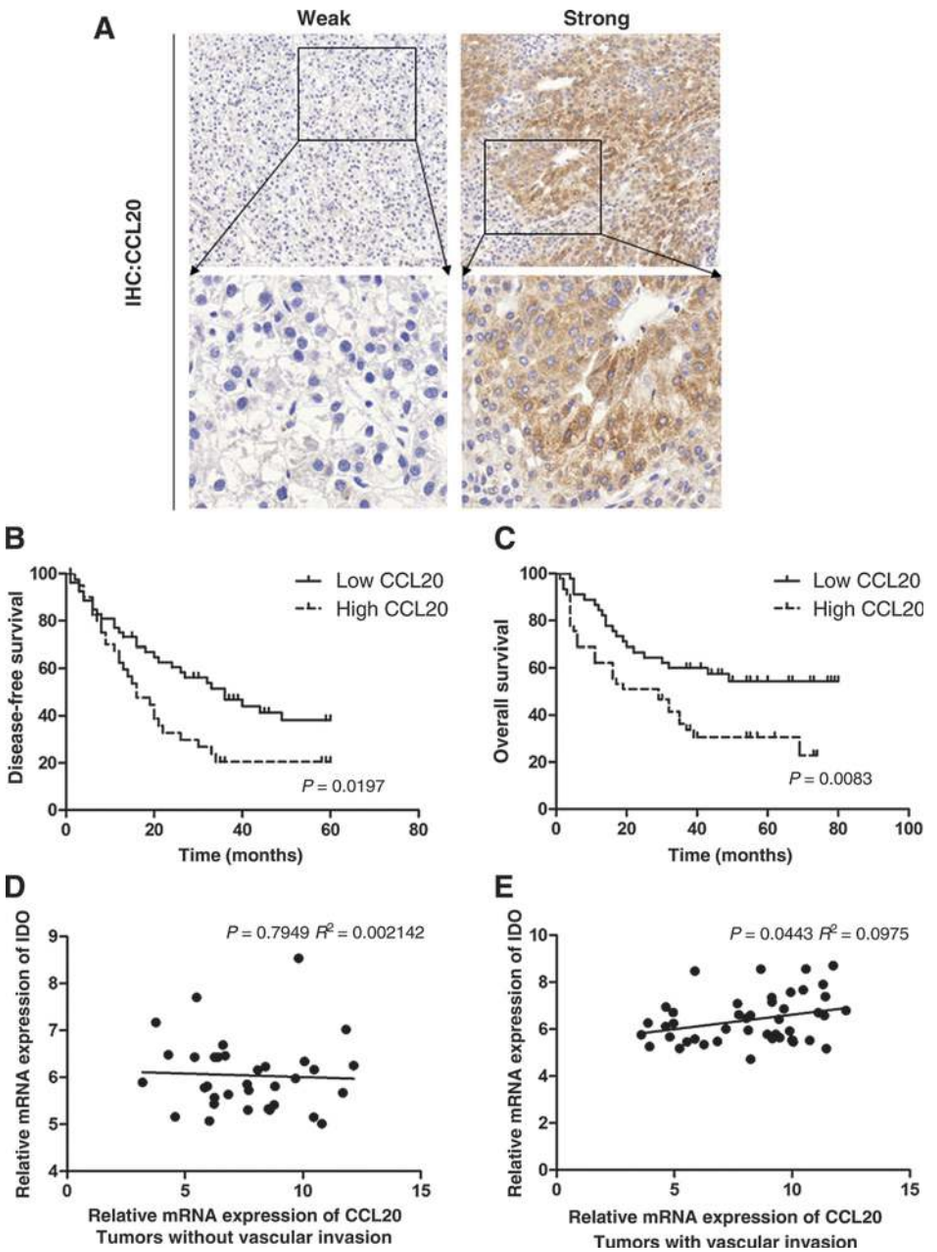

Figure 6.
High amounts of CCL20 are predictive of poor patient survival. A, hepatocellular carcinoma tissue sections ($n = 90$) were stained with an antibody against CCL20. Representative images (magnification, ×200) from a patient with "low" (weak) CCL20 levels and from a patient with "high" (strong) CCL20 levels are shown. Lower panel represents magnified views (×400) indicated by boxes in the top panel. B and C, the disease-free survival and cumulative overall survival of hepatocellular carcinoma patients with high or low CCL20 expression levels (based on median CCL20 levels) estimated using the Kaplan–Meier method and compared by the log-rank test in the same set of patients. D and E, the relationship between CCL20 and IDO expression in hepatocellular carcinoma patients without and with vascular invasion from the National Centre for Biotechnology Information Gene Expression Omnibus database (GSE20238) assessed by linear regression.

Among the cytokines upregulated during hypoxic EMT, CCL20 was required for the induction of IDO expression in monocyte-derived macrophages. Indeed, the analysis of our clinical samples showed that CCL20 was significantly associated with IDO expression in hepatocellular carcinoma with PVTT. Moreover, as monocyte-derived macrophages are typically composed of three subsets, which are characterized by different levels of CD14 and CD16 expression, we assessed whether they showed differential responses to the hypoxia. We showed that all three subsets of monocytes could be affected by our coculture system. Although the subsets showed differential expression of CD163 and CD206, they all showed increased IDO expression. Therefore, CCl20 is required for the induction of IDO expression in monocyte-derived macrophages.

Previous studies showed that the CCL20–CCR6 axis is important for the recruitment of circulating T_{regs} into the tumor microenvironment (43). Here, we demonstrated that CCL20-treated IDO^+ monocyte-derived macrophages significantly inhibited the T-cell proliferative activity compared with untreated monocyte-derived macrophages in an IDO-dependent way. Inhibition of IDO activity by 1-MT significantly attenuated monocyte-derived macrophage–mediated suppression on T-cell proliferation and production of IFNγ in $CD4^+$ and $CD8^+$ cells. On the other hand, we found the $CD25^+Foxp3^+$ T_{reg}-like cells significantly increased in samples cultured with CCL20-treated IDO^+ monocyte-derived

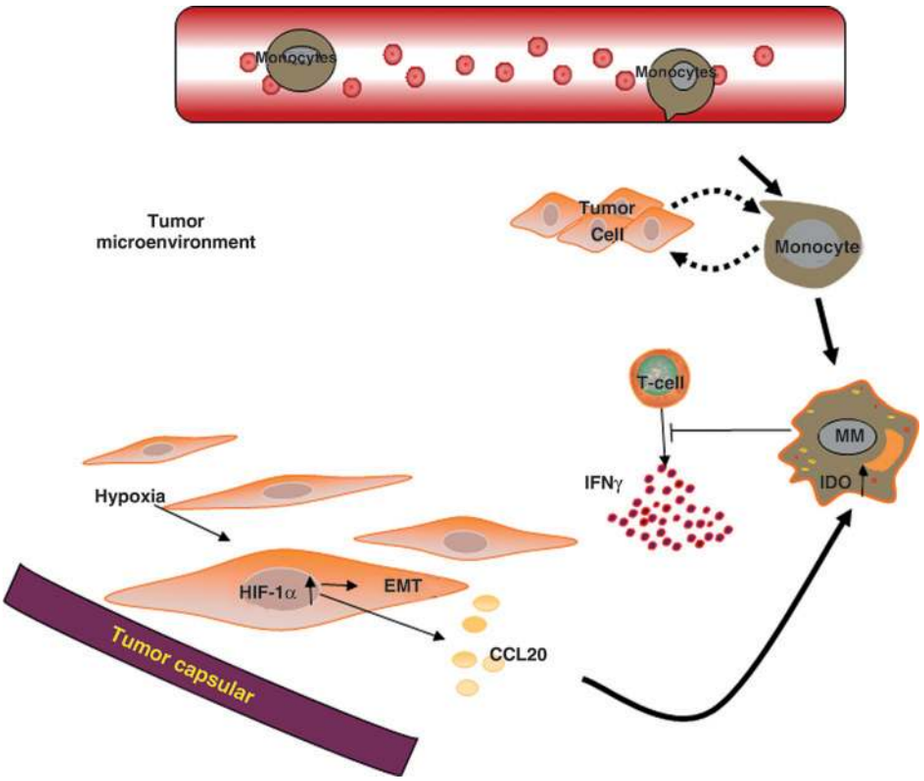

Figure 7.
Schematic model depicting the cancer cell and monocyte-derived macrophage cross-talk observed in the tumor microenvironment. When the circulating monocytes are recruited to the tumor, cancer cells educate them, converting them into monocyte-derived macrophages. After the hypoxia-induced EMT of cancer cells located in the invasive front, the transitioned cells will secret CCL20, which, in turn, induces IDO upregulation in the monocyte-derived macrophages. This subset of IDO^+ monocyte-derived macrophages counteract effective T-cell responses by inhibiting the proliferation of T cells and the production of IFNγ.

macrophages compared with those cultured with untreated monocyte-derived macrophages. The potential mechanism for the increase in $CD25^+Foxp3^+$ T_{reg}-like cells may be the production of TGFβ, IL10, and thrombospondin-1 (TSP1), which have been reported to induce T_{regs} (44, 45). Together, these results indicate that the release of CCL20 during hypoxic–EMT plays an important role in creating a tumor immunosuppressive microenvironment.

In macrophages and DCs, STAT1 activation has been shown to induce IDO expression via type I or type II IFN stimulation (46). In addition, posttranslational modification of STAT3 by phosphorylation and/or acetylation has been demonstrated to be essential for the expression of IDO in DCs in response to commensal bacteria or allograft transplant (47–49). In this study, we examined the expression and phosphorylation of STAT1 and STAT3 and found that the level of pSTAT1, but not pSTAT3, significantly increased in CCL20-treated monocyte-derived macrophages. This suggests that CCL20 induced expression of IDO might be due to phosphorylation of STAT1. Therefore, CCL20 may act in similar way to the classical IFNγ signaling pathway that has previously been reported to increase IDO expression.

Macrophages are versatile, plastic cells that can respond to environmental signals and differentiate into a tumor supportive phenotype (24, 50). Several studies identified the interaction between cancer cells and macrophages, using condition medium from cancer cell line to induce macrophages (22, 33). However, these studies may not reflect the real status in a tumor microenvironment, where they would be in direct cell-to-cell contact. Therefore, it is likely that this induction effect will be reduced if the cancer and immune cells are separately cultured. To mimic a hepatocellular carcinoma cell condition microenvironment *in vitro*, we cocultured monocytes with hepatoma cells. We found that IDO was weakly expressed in the monocyte-derived macrophages after coculture with hepatoma cells, and there was no IDO expression in macrophages induced by the condition medium alone (33).

In conclusion, our results provide new insights into the action of CCL20 on monocyte-derived macrophages that was exercised to counteract effective T-cell responses. The hypoxia-induced EMT of cancer cells helps to educate newly recruited monocytes by secreting CCL20, which leads to IDO upregulation in the monocytes. This suppressive IDO^+ monocyte-derived macrophages, act to suppress T-cell responses and promote to tolerance to tumor antigens. In this way, IDO^+ monocyte-derived macrophages create immunosuppressive conditions in the tumor microenvironment and promote metastasis (Fig. 7). As elevated CCL20 levels were associated with a poor prognosis in hepatocellular carcinoma patients, preventing CCL20 elevation may stop the creation of an immunosuppressive tumor microenvironment and slow metastasis. Therefore, targeting CCL20 may be a promising strategy for treating human hepatocellular carcinoma in the future.

Disclosure of Potential Conflicts of Interest

No potential conflicts of interest were disclosed.

Authors' Contributions

Conception and design: L.-Y. Ye, W. Chen, Q. Zhang, T.-B. Liang
Development of methodology: L.-Y. Ye, Q. Zhang, T.-B. Liang

Acquisition of data (provided animals, acquired and managed patients, provided facilities, etc.): L.-Y. Ye, W. Chen, X.-L. Bai, Q. Zhang
Analysis and interpretation of data (e.g., statistical analysis, biostatistics, computational analysis): L.-Y. Ye, X.-L. Bai, Q. Zhang, Q.-D. Hu
Writing, review, and/or revision of the manuscript: L.-Y. Ye, W. Chen, X.-L. Bai, X.-Y. Xu, Q. Zhang, X.-F. Xia, G.-G. Li, Q.-D. Hu, Q.-H. Fu
Administrative, technical, or material support (i.e., reporting or organizing data, constructing databases): L.-Y. Ye, X.-L. Bai, X.-Y. Xu, Q. Zhang, X. Sun, Q.-D. Hu, T.-B. Liang
Study supervision: L.-Y. Ye, T.-B. Liang

Grant Support

This study was supported by grants from the National High Technology Research and Development Program 863 of China (SS2015AA020405 to T.B. Liang; and SS2014AA020533, to W. Chen) and National Natural Science Foundation of China (81472212 to T.B. Liang; 91442115 to X.L. Bai; 81130007 to T.B. Liang; 81302071 to W. Chen; 81401954 to Q. Zhang; and 81171884 to X.L. Bai).

Received April 15, 2015; revised October 2, 2015; accepted October 20, 2015; published OnlineFirst February 2, 2016.

References

1. Lau WY. Management of hepatocellular carcinoma. J R Coll Surg 2002;47:389–99.
2. Parkin DM, Bray F, Ferlay J, Pisani P. Global cancer statistics, 2002. CA Cancer J Clin 2005;55:74–108.
3. Kim Y, Ejaz A, Tayal A, Spolverato G, Bridges JF, Anders RA, et al. Temporal trends in population-based death rates associated with chronic liver disease and liver cancer in the United States over the last 30 years. Cancer 2014;120:3058–65.
4. Wu CC, Hsieh SR, Chen JT, Ho WL, Lin MC, Yeh DC, et al. An appraisal of liver and portal vein resection for hepatocellular carcinoma with tumor thrombi extending to portal bifurcation. Arch Surg 2000;135: 1273–9.
5. Chen XP, Qiu FZ, Wu ZD, Zhang ZW, Huang ZY, Chen YF, et al. Effects of location and extension of portal vein tumor thrombus on long-term outcomes of surgical treatment for hepatocellular carcinoma. Ann Surg Oncol 2006;13:940–6.
6. Ohkubo T, Yamamoto J, Sugawara Y, Shimada K, Yamasaki S, Makuuchi M, et al. Surgical results for hepatocellular carcinoma with macroscopic portal vein tumor thrombosis. J Am Coll Surg 2000;191:657–60.
7. Shi J, Lai EC, Li N, Guo WX, Xue J, Lau WY, et al. Surgical treatment of hepatocellular carcinoma with portal vein tumor thrombus. Ann Surg Oncol 2010;17:2073–80.
8. Yuki K, Hirohashi S, Sakamoto M, Kanai T, Shimosato Y. Growth and spread of hepatocellular carcinoma. A review of 240 consecutive autopsy cases. Cancer 1990;66:2174–9.
9. Le Treut YP, Hardwigsen J, Ananian P, Saisse J, Gregoire E, Richa H, et al. Resection of hepatocellular carcinoma with tumor thrombus in the major vasculature. A European case-control series. J Gastrointest Surg 2006;10: 855–62.
10. Pawlik TM, Poon RT, Abdalla EK, Ikai I, Nagorney DM, Belghiti J, et al. Hepatectomy for hepatocellular carcinoma with major portal or hepatic vein invasion: results of a multicenter study. Surgery 2005;137: 403–10.
11. Schoenleber SJ, Kurtz DM, Talwalkar JA, Roberts LR, Gores GJ. Prognostic role of vascular endothelial growth factor in hepatocellular carcinoma: systematic review and meta-analysis. Br J Cancer 2009;100:1385–92.
12. Kanda M, Nomoto S, Nishikawa Y, Sugimoto H, Kanazumi N, Takeda S, et al. Correlations of the expression of vascular endothelial growth factor B and its isoforms in hepatocellular carcinoma with clinico-pathological parameters. J Surg Oncol 2008;98:190–6.
13. Tlsty TD, Coussens LM. Tumor stroma and regulation of cancer development. Ann Rev Pathol 2006;1:119–50.
14. Wong CC, Tse AP, Huang YP, Zhu YT, Chiu DK, Lai RK, et al. Lysyl oxidase-like 2 is critical to tumor microenvironment and metastatic niche formation in hepatocellular carcinoma. Hepatology 2014;60:1645–58.
15. Lundgren K, Nordenskjold B, Landberg G. Hypoxia, Snail and incomplete epithelial-mesenchymal transition in breast cancer. Br J Cancer 2009;101: 1769–81.
16. Scheel C, Onder T, Karnoub A, Weinberg RA. Adaptation versus selection: the origins of metastatic behavior. Cancer Res 2007;67:11476–9.
17. Brabletz T, Jung A, Reu S, Porzner M, Hlubek F, Kunz-Schughart LA, et al. Variable beta-catenin expression in colorectal cancers indicates tumor progression driven by the tumor environment. Proc Natl Acad Sci U S A 2001;98:10356–61.
18. Brabletz T. To differentiate or not–routes towards metastasis. Nat Rev Cancer 2012;12:425–36.
19. Hernandez L, Smirnova T, Kedrin D, Wyckoff J, Zhu L, Stanley ER, et al. The EGF/CSF-1 paracrine invasion loop can be triggered by heregulin beta1 and CXCL12. Cancer Res 2009;69:3221–7.
20. Su S, Liu Q, Chen J, Chen F, He C, Huang D, et al. A positive feedback loop between mesenchymal-like cancer cells and macrophages is essential to breast cancer metastasis. Cancer Cell 2014;25:605–20.
21. Kuang DM, Peng C, Zhao Q, Wu Y, Chen MS, Zheng L. Activated monocytes in peritumoral stroma of hepatocellular carcinoma promote expansion of memory T helper 17 cells. Hepatology 2010;51:154–64.
22. Kuang DM, Zhao Q, Peng C, Xu J, Zhang JP, Wu C, et al. Activated monocytes in peritumoral stroma of hepatocellular carcinoma foster immune privilege and disease progression through PD-L1. J Exp Med 2009;206:1327–37.
23. Lewis CE, Pollard JW. Distinct role of macrophages in different tumor microenvironments. Cancer Res 2006;66:605–12.
24. Gordon S, Taylor PR. Monocyte and macrophage heterogeneity. Nat Rev Immunol 2005;5:953–64.
25. Mellor AL, Munn DH. IDO expression by dendritic cells: tolerance and tryptophan catabolism. Nat Rev Immunol 2004;4:762–74.
26. Chen BW, Chen W, Liang H, Liu H, Liang C, Zhi X, et al. Inhibition of mTORC2 induces cell-cycle arrest and enhances the cytotoxicity of doxorubicin by suppressing MDR1 expression in HCC cells. Mol Cancer Therap 2015;14:1805–15.
27. Forsythe JA, Jiang BH, Iyer NV, Agani F, Leung SW, Koos RD, et al. Activation of vascular endothelial growth factor gene transcription by hypoxia-inducible factor 1. Mol Cell Biol 1996;16:4604–13.
28. Matin A, Streete IM, Jamie IM, Truscott RJ, Jamie JF. A fluorescence-based assay for indoleamine 2,3-dioxygenase. Anal Biochem 2006;349:96–102.
29. Zhu XD, Zhang JB, Zhuang PY, Zhu HG, Zhang W, Xiong YQ, et al. High expression of macrophage colony-stimulating factor in peritumoral liver tissue is associated with poor survival after curative resection of hepatocellular carcinoma. J Clin Oncol 2008;26:2707–16.
30. Blouin CC, Page EL, Soucy GM, Richard DE. Hypoxic gene activation by lipopolysaccharide in macrophages: implication of hypoxia-inducible factor 1alpha. Blood 2004;103:1124–30.
31. Hatano N, Itoh Y, Suzuki H, Muraki Y, Hayashi H, Onozaki K, et al. Hypoxia-inducible factor-1alpha (HIF1alpha) switches on transient receptor potential ankyrin repeat 1 (TRPA1) gene expression via a hypoxia response element-like motif to modulate cytokine release. J Biol Chem 2012;287:31962–72.
32. Tong Y, Li QG, Xing TY, Zhang M, Zhang JJ, Xia Q. HIF1 regulates WSB-1 expression to promote hypoxia-induced chemoresistance in hepatocellular carcinoma cells. FEBS Lett 2013;587:2530–5.
33. Zhao Q, Kuang DM, Wu Y, Xiao X, Li XF, Li TJ, et al. Activated CD69+ T cells foster immune privilege by regulating IDO expression in tumor-associated macrophages. J Immunol 2012;188:1117–24.
34. Ziegler-Heitbrock L, Ancuta P, Crowe S, Dalod M, Grau V, Hart DN, et al. Nomenclature of monocytes and dendritic cells in blood. Blood 2010;116: e74–80.
35. Moniuszko M, Bodzenta-Lukaszyk A, Kowal K, Lenczewska D, Dabrowska M. Enhanced frequencies of CD14++CD16+, but not CD14+CD16+, peripheral blood monocytes in severe asthmatic patients. Clin Immunol 2009;130:338–46.
36. Auffray C, Sieweke MH, Geissmann F. Blood monocytes: development, heterogeneity, and relationship with dendritic cells. Annu Rev Immunol 2009;27:669–92.

37. Minguez B, Hoshida Y, Villanueva A, Toffanin S, Cabellos L, Thung S, et al. Gene-expression signature of vascular invasion in hepatocellular carcinoma. J Hepatol 2011;55:1325–31.
38. Lanzen J, Braun RD, Klitzman B, Brizel D, Secomb TW, Dewhirst MW. Direct demonstration of instabilities in oxygen concentrations within the extravascular compartment of an experimental tumor. Cancer Res 2006;66:2219–23.
39. Rofstad EK, Galappathi K, Mathiesen B, Ruud EB. Fluctuating and diffusion-limited hypoxia in hypoxia-induced metastasis. Clin Cancer Res 2007;13:1971–8.
40. Zeisberg M, Neilson EG. Biomarkers for epithelial-mesenchymal transitions. J Clin Invest 2009;119:1429–37.
41. Singh A, Settleman J. EMT, cancer stem cells and drug resistance: an emerging axis of evil in the war on cancer. Oncogene 2010;29:4741–51.
42. Kudo-Saito C, Shirako H, Takeuchi T, Kawakami Y. Cancer metastasis is accelerated through immunosuppression during Snail-induced EMT of cancer cells. Cancer Cell 2009;15:195–206.
43. Chen KJ, Lin SZ, Zhou L, Xie HY, Zhou WH, Taki-Eldin A, et al. Selective recruitment of regulatory T cell through CCR6-CCL20 in hepatocellular carcinoma fosters tumor progression and predicts poor prognosis. PLoS One 2011;6:e24671.
44. Futagami Y, Sugita S, Vega J, Ishida K, Takase H, Maruyama K, et al. Role of thrombospondin-1 in T cell response to ocular pigment epithelial cells. J Immunol 2007;178:6994–7005.
45. von Boehmer H. Mechanisms of suppression by suppressor T cells. Nat Immunol 2005;6:338–44.
46. Chon SY, Hassanain HH, Gupta SL. Cooperative role of interferon regulatory factor 1 and p91 (STAT1) response elements in interferon-gamma-inducible expression of human indoleamine 2,3-dioxygenase gene. J Biol Chem 1996;271:17247–52.
47. Barton BE. STAT3: a potential therapeutic target in dendritic cells for the induction of transplant tolerance. Expert Opin Ther Targets 2006;10:459–70.
48. Bonifazi P, Zelante T, D'Angelo C, De Luca A, Moretti S, Bozza S, et al. Balancing inflammation and tolerance in vivo through dendritic cells by the commensal Candida albicans. Mucosal Immunol 2009;2:362–74.
49. Poschke I, Mougiakakos D, Hansson J, Masucci GV, Kiessling R. Immature immunosuppressive CD14+HLA-DR-/low cells in melanoma patients are Stat3hi and overexpress CD80, CD83, and DC-sign. Cancer Res 2010;70:4335–45.
50. Mantovani A, Sozzani S, Locati M, Allavena P, Sica A. Macrophage polarization: tumor-associated macrophages as a paradigm for polarized M2 mononuclear phagocytes. Trends Immunol 2002;23:549–55.